Dielectric Profile of Interfacial Water and its Effect on Double-Layer Capacitance

Douwe Jan Bonthuis,[1] Stephan Gekle,[1] and Roland R. Netz[2]

[1]*Physik Department, Technische Universität München, 85748 Garching, Germany*

[2]*Fachbereich Physik, Freie Universität, Berlin, 14195 Berlin, Germany*

(Received 5 April 2011; revised manuscript received 25 May 2011; published 13 October 2011)

The framework for deriving tensorial interfacial dielectric profiles from bound charge distributions is established and applied to molecular dynamics simulations of water at hydrophobic and hydrophilic surfaces. In conjunction with a modified Poisson-Boltzmann equation, the trend of experimental double-layer capacitances is well reproduced. We show that the apparent Stern layer can be understood in terms of the dielectric profile of pure water.

DOI: 10.1103/PhysRevLett.107.166102 PACS numbers: 68.08.−p, 77.22.Ch, 61.20.Ja

One of the most salient properties of water is its high molecular polarity. As a result, electrostatic interactions in aqueous environments are drastically modified with profound implications for the behavior of ions, proteins, and membranes in solution [1]. Experiments and simulations have shown that the dielectric function of homogeneous water exhibits two singularities for wave vectors at molecular length scales, indicating anomalous screening effects in bulk [2]. To what extent interfacial water exhibits similar anomalies is less clear [3]. Experimental capacitance studies have led Stern to propose a model for an aqueous interface where the dielectric constant is reduced over a nanoscopic width [4]. Whether this layer reflects ionic or rather intrinsic water properties is not specified in the original Stern model. However, recent terahertz spectroscopy experiments have shown that the dielectric properties of water itself are modified at interfaces within a layer of molecular size [5]. Without considering an explicit interfacial dielectric profile, the relation between the nonlocal dielectric function and the Stern layer contribution to the capacitance has been established [6] including nonlinear effects [7]. Using approximate statistical mechanical methods, the decrease of the interfacial capacitance for a dipolar fluid has been related to molecular ordering and orientation [8]. However, a method for extracting dielectric profiles from interfacial water orientational and spatial distributions, as well as detailed knowledge of the profiles themselves, have been lacking so far.

A thorough understanding of the interfacial dielectric behavior of water is a prerequisite for correct modeling of ion distributions [9] and double-layer interactions [10], as well as electrokinetic effects. Similarly, the interfacial dielectric function is a key ingredient to solvent-implicit approaches toward protein and macromolecular modeling [11]. Control over the interfacial dielectric constant is also crucial for a number of industrial applications, including high power and long duration energy storage devices [12]. Finally, dielectric effects are one contribution to the hydration repulsion between polar surfaces [1,13]. The dielectric properties of interfacial water have been studied using both simulations and analytic approaches. One shortcoming of previous analytic approaches is that the water bulk behavior, including the above-mentioned anomaly, is typically not accounted for [14,15]. At the same time, previous simulations with explicit water and ions could not be analyzed within the existing theoretical framework. One reason for the complexity is the appearance of higher order multipole moments, which are particularly essential at interfaces [16].

The purpose of this Letter is threefold: First, we develop the theoretical framework to extract both parallel and perpendicular interfacial dielectric response functions from the bound charge distribution. Quadrupole and higher order moments, which were neglected previously [17], turn out to be crucial. Second, we extract the dielectric response functions using large-scale molecular dynamics (MD) simulations of water and demonstrate that the perpendicular dielectric function exhibits singularities like the nonlocal bulk dielectric function, whereas the parallel function is smooth. The remarkable differences between hydrophobic and hydrophilic surfaces can be quantified in terms of a dielectric dividing surface, defined similarly to the Gibbs dividing surface. Third, we use a modified Poisson-Boltzmann equation to show that the experimental double-layer capacitance can be largely understood by the dielectric profile of pure water.

Dielectric linear response.—A local change in displacement field $\boldsymbol{D}(\boldsymbol{r})$ is related to a change in electric field $\boldsymbol{E}(\boldsymbol{r}')$ via the nonlocal dielectric tensor $\varepsilon_{\mathrm{nl}}(\boldsymbol{r},\boldsymbol{r}')$, $\Delta\boldsymbol{D}(\boldsymbol{r}) = \varepsilon_0 \int \varepsilon_{\mathrm{nl}}(\boldsymbol{r},\boldsymbol{r}') \cdot \Delta\boldsymbol{E}(\boldsymbol{r}')d\boldsymbol{r}'$, with ε_0 the permittivity of vacuum. For a homogeneous electric field, $\Delta\boldsymbol{E}(\boldsymbol{r}) = \Delta\boldsymbol{E}$, which holds for the averaged tangential field component at planar interfaces as will be discussed below, the response function becomes local,

$$\Delta\boldsymbol{D}(\boldsymbol{r}) = \varepsilon_0 \varepsilon(\boldsymbol{r}) \cdot \Delta\boldsymbol{E}, \tag{1}$$

with $\varepsilon(\boldsymbol{r}) = \int \varepsilon_{\mathrm{nl}}(\boldsymbol{r},\boldsymbol{r}')d\boldsymbol{r}'$. This makes the usual locality assumption $\varepsilon_{\mathrm{nl}}(\boldsymbol{r},\boldsymbol{r}') = \varepsilon(\boldsymbol{r})\delta(\boldsymbol{r}-\boldsymbol{r}')$ superfluous. The inverse response function $\varepsilon_{\mathrm{nl}}^{-1}(\boldsymbol{r},\boldsymbol{r}')$ is defined by $\Delta\boldsymbol{E}(\boldsymbol{r}) = \varepsilon_0^{-1} \int \varepsilon_{\mathrm{nl}}^{-1}(\boldsymbol{r},\boldsymbol{r}') \cdot \Delta\boldsymbol{D}(\boldsymbol{r}')d\boldsymbol{r}'$ [6] and becomes local when

 © 2011 American Physical Society

$\boldsymbol{D}(\boldsymbol{r})$ is uniform, which holds for the averaged perpendicular component at a planar interface,

$$\Delta \boldsymbol{E}(\mathbf{r}) = \varepsilon_0^{-1}\varepsilon^{-1}(\mathbf{r}) \cdot \Delta \boldsymbol{D}, \tag{2}$$

with $\varepsilon^{-1}(\boldsymbol{r})$ the inverse dielectric function.

Fluctuation-dissipation relation.—The electric field is separated into the displacement field $\boldsymbol{D}(\boldsymbol{r})$, associated with the monopole density, and the polarization $\boldsymbol{m}(\boldsymbol{r})$ generated by all higher multipole moments, $\varepsilon_0 \boldsymbol{E}(\boldsymbol{r}) = \boldsymbol{D}(\boldsymbol{r}) - \boldsymbol{m}(\boldsymbol{r})$. Defining the total polarization in a volume $\mathcal{V}$ by $\boldsymbol{M} = \int_{\mathcal{V}} \boldsymbol{m}(\boldsymbol{r}) d\boldsymbol{r}$, the change in polarization upon application of an external homogeneous electric field $\boldsymbol{F}$, defined as $\Delta \boldsymbol{m}(\boldsymbol{r}) = \langle \boldsymbol{m}(\boldsymbol{r}) \rangle_{\boldsymbol{F}} - \langle \boldsymbol{m}(\boldsymbol{r}) \rangle_0$, is given by [17,18]

$$\Delta \boldsymbol{m} = \frac{\int (\boldsymbol{m} - \langle \boldsymbol{m} \rangle_0) \exp[-\beta(U - \boldsymbol{M} \cdot \boldsymbol{F})] dX}{\int \exp[-\beta(U - \boldsymbol{M} \cdot \boldsymbol{F})] dX}, \tag{3}$$

where $\langle \cdots \rangle_{\boldsymbol{F}}$ and $\langle \cdots \rangle_0$ denote ensemble averages in the presence and absence of $\boldsymbol{F}$, respectively, β is the inverse thermal energy and dX denotes phase space integration. For small $\boldsymbol{F}$, Eq. (3) can be linearized to yield

$$\Delta \boldsymbol{m}(\boldsymbol{r}) \approx \beta [\langle \boldsymbol{m}(\boldsymbol{r}) \boldsymbol{M} \rangle_0 - \langle \boldsymbol{m}(\boldsymbol{r}) \rangle_0 \langle \boldsymbol{M} \rangle_0] \cdot \boldsymbol{F}. \tag{4}$$

Slab geometry.—We consider a planar interfacial system with translational invariance in the x and y directions, so all averaged fields and observables only depend on z. The dielectric tensor is diagonal with only two unique components, parallel and perpendicular to the surface. Maxwell's equation $\boldsymbol{\nabla} \times \mathbf{E}(z) = 0$ implies $\Delta E_{\parallel}(z) = E_{\parallel}$, which shows that the tangential electric field is constant on average, i.e., neglecting field fluctuations due to, e.g., local water orientations. Equation (1) applies to this situation, yielding the parallel dielectric response

$$\varepsilon_{\parallel}(z) = 1 + \frac{\Delta m_{\parallel}(z)}{\varepsilon_0 E_{\parallel}}. \tag{5}$$

The homogeneous field $F_{\parallel}$ in Eq. (4) corresponds to $E_{\parallel}$ in the parallel case. Combining Eqs. (4) and (5) gives

$$\varepsilon_{\parallel}(z) \approx 1 + \varepsilon_0^{-1} \beta [\langle m_{\parallel}(z) M_{\parallel} \rangle_0 - \langle m_{\parallel}(z) \rangle_0 \langle M_{\parallel} \rangle_0]. \tag{6}$$

For vanishing monopole density we have $\nabla \cdot \boldsymbol{D}(z) = 0$ and thus the averaged perpendicular displacement field is constant, $\Delta D_{\perp}(z) = D_{\perp}$. To this case, Eq. (2) applies and the perpendicular dielectric response follows as

$$\varepsilon_{\perp}^{-1}(z) = 1 - \frac{\Delta m_{\perp}(z)}{D_{\perp}}. \tag{7}$$

The field $F_{\perp}$ is associated with $D_{\perp}/\varepsilon_0$. Combining Eqs. (4) and (7) yields

$$\varepsilon_{\perp}^{-1}(z) \approx 1 - \varepsilon_0^{-1} \beta [\langle m_{\perp}(z) M_{\perp} \rangle_0 - \langle m_{\perp}(z) \rangle_0 \langle M_{\perp} \rangle_0]. \tag{8}$$

Whereas $\varepsilon_{\parallel}(z)$ is irrelevant for planar systems with lateral translational invariance, it becomes crucial for the dielectric response of, e.g., a point charge at an interface.

Simulations and results.—We perform MD simulations (GROMACS) of pure SPC/E water in contact with two diamond surface types, one terminated with hydroxyl groups (surface coverage $x_{\mathrm{OH}} = 1/4$ in the notation of [19]), giving a hydrophilic surface, and one terminated with hydrogen atoms, giving a hydrophobic surface (see [19] for simulation details). Snapshots of the simulations are shown in Fig. 1, together with the number density profiles. Notably, the water density peak at the hydrophilic surface is significantly higher than at the hydrophobic surface. We calculate the dielectric response in two distinct ways: First, from polarization fluctuations without an external electric field using Eqs. (6) and (8), and second, directly from Eqs. (5) and (7) at a finite field $\boldsymbol{F}$ (for which the response is *a posteriori* verified to be linear). To get the excess polarization $\Delta \boldsymbol{m}(\boldsymbol{r})$, the polarization at $\boldsymbol{F} = 0$ is subtracted.

The parallel dielectric profile $\varepsilon_{\parallel}(z)$ is shown in Fig. 2 for a hydrophilic (a) and a hydrophobic surface (b). Solid lines depict results at vanishing external field using Eq. (6), while dashed lines follow from Eq. (5) for an external electric field of $F_{\parallel} = E_{\parallel} = 0.05$ V/nm. The parallel polarization profile $m_{\parallel}(z)$ is calculated directly from the boundary charge created by introducing virtual cuts in the simulation box, which is shown to be equivalent to a summation over all multipole moments [18]. The bulk dielectric response is close to the literature value for SPC/E water of $\varepsilon_{\mathrm{bulk}} = 71$ [20], and the profiles from fluctuations and the applied field coincide excellently. Clearly, the dielectric profiles are roughly proportional to the density profiles. This is typically assumed in coarse-grained solvation models [11], but strictly valid only for noninteracting systems. Interestingly, however, the

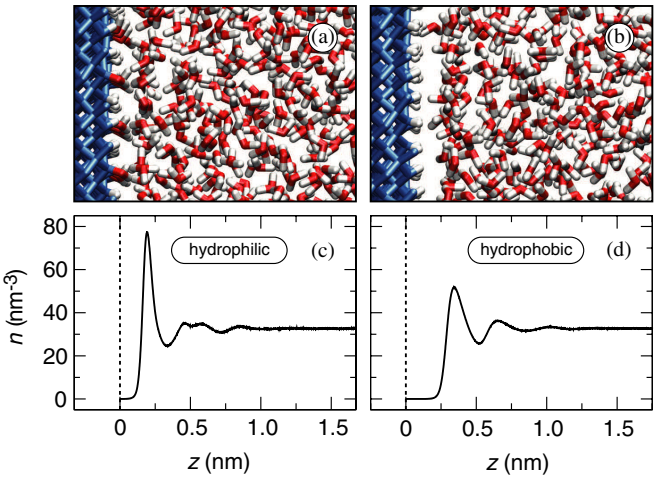

FIG. 1 (color online). Snapshots from the simulations of the (a) hydrophilic and (b) hydrophobic surfaces and (c)–(d) corresponding water density profiles $n(z)$ without an external electric field. All graphs have the same z scale, with $z = 0$ fixed at the outermost carbon atoms for the hydrophobic and at the oxygen atoms of the hydroxyl groups for the hydrophilic surface.

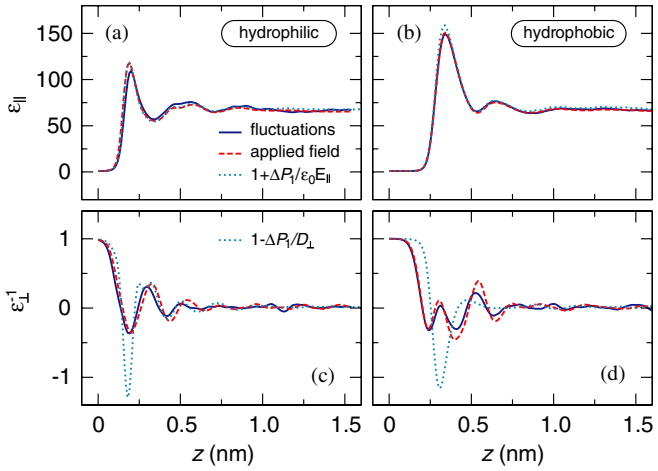

FIG. 2 (color online). The parallel dielectric function $\varepsilon_\parallel$ next to a (a) hydrophilic and a (b) hydrophobic diamond calculated from polarization fluctuations [Eq. (6), solid lines] and for an external electric field $E_\parallel = 0.05$ V/nm [Eq. (5), dashed lines]. The inverse perpendicular dielectric function $\varepsilon_\perp^{-1}$ next to a (c) hydrophilic and a (d) hydrophobic diamond from fluctuations [Eq. (8), solid lines] and for an external electric field $D_\perp/\varepsilon_0 = \pm 0.5$ V/nm [Eq. (7), dashed lines]. The dotted lines denote the dipole contribution for an applied external field.

dielectric peak is higher at the hydrophobic surface compared to the hydrophilic surface, in contrast to the density, which shows the opposite trend. This disparity indicates that, although there are more polarizable molecules available in the first density peak at the hydrophilic surface, their response to an electric field is more restricted than at the hydrophobic surface. This points to a fundamental difference in dielectric response between the two surfaces, which we will get back to later. Shown as dotted lines are the dipolar dielectric contributions, calculated using only the excess dipole density $\Delta \boldsymbol{P}_1(z)$ instead of the total excess polarization $\Delta \boldsymbol{m}(z)$, which agree perfectly with the full $\varepsilon_\parallel(z)$ profiles, showing that quadrupole and higher order contributions are negligible for the parallel response.

The inverse perpendicular dielectric profile is shown in Fig. 2 at a hydrophilic (c) and a hydrophobic surface (d). We calculate $m_\perp(z)$ directly from the total charge density $\rho(z)$ via $m_\perp(z) = -\int_0^z \rho(z')dz'$. Solid lines show the response calculated from fluctuations using Eq. (8), and dashed curves represent the response to an applied electric field of ± 0.5 V/nm from Eq. (7). Again, both computational methods agree, thus confirming our formalism. Strikingly, $\varepsilon_\perp^{-1}(z)$ passes through zero several times, meaning that $\varepsilon_\perp(z)$ exhibits multiple singularities and extensive negative parts. This overscreening behavior is reminiscent of the nonlocal bulk dielectric function [2], which evidently dominates the dielectric response perpendicular to the surface, but not the parallel one. In contrast with the parallel case, the dipolar dielectric contributions (dotted lines) deviate from the full $\varepsilon_\perp^{-1}(z)$ profiles, showing that here quadrupole and higher order terms are crucial. This vividly illustrates shortcomings of previous formulations [17]. Although $\varepsilon_\perp^{-1}(z)$ must be related to the molecular ordering, there is no direct correlation between $\varepsilon_\perp^{-1}(z)$ and the electric field stemming from the oriented molecules [18].

Dielectric dividing surface.—To interpret and apply our simulation results in a transparent fashion, we introduce the dielectric dividing surface position z^{DDS}, in analogy to the Gibbs dividing surface defined by

$$z^{\mathrm{DDS}} = z_v + \int_{z_v}^{z_l} \frac{f(z_l) - f(z)}{f(z_l) - f(z_v)} dz, \tag{9}$$

where z_v and z_l are positions in the vapor and liquid phases, respectively. For the Gibbs dividing surface z^{GDS}, $f(z)$ is the fluid number density $n(z)$, and we obtain $z^{\mathrm{GDS}}_{\mathrm{phob}} = 0.22$ nm and $z^{\mathrm{GDS}}_{\mathrm{phil}} = 0.07$ nm, reflecting the well-known tendency for water to form a pronounced depletion layer at hydrophobic surfaces [19]. For the dielectric dividing surfaces $z^{\mathrm{DDS}}_\parallel$ and $z^{\mathrm{DDS}}_\perp$, we take $f(z) = \varepsilon_\parallel(z)$ and $f(z) = \varepsilon_\perp^{-1}(z)$, respectively, giving $z^{\mathrm{DDS}}_{\parallel\mathrm{phil}} = 0.09$ nm, $z^{\mathrm{DDS}}_{\parallel\mathrm{phob}} = 0.08$ nm, $z^{\mathrm{DDS}}_{\perp\mathrm{phil}} = 0.10$ nm, and $z^{\mathrm{DDS}}_{\perp\mathrm{phob}} = 0.12$ nm. Using a previous dielectric layer definition [7] together with our $\varepsilon_\perp^{-1}(z)$, we obtain $z_{\perp\mathrm{phil}} = 0.08$ nm and $z_{\perp\mathrm{phob}} = 0.12$ nm, which is not very different from $z^{\mathrm{DDS}}_\perp$. Note that by construction, our definition of the dielectric dividing surface position combined with a sharp-kink approximation, $\varepsilon_\perp^{-1}(z) = 1$ for $z < z^{\mathrm{DDS}}_\perp$ and $\varepsilon_\perp^{-1}(z) = \varepsilon^{-1}_{\mathrm{bulk}}$ otherwise, ensures the correct asymptotic voltage profile far away from the interface. For the dielectric shifts, defined as $\delta_\parallel = z^{\mathrm{DDS}}_\parallel - z^{\mathrm{GDS}}$ and $\delta_\perp = z^{\mathrm{DDS}}_\perp - z^{\mathrm{GDS}}$, we obtain $\delta^{\mathrm{phil}}_\parallel = 0.02 \pm 0.01$ nm and $\delta^{\mathrm{phil}}_\perp = 0.03 \pm 0.015$ nm at the hydrophilic and $\delta^{\mathrm{phob}}_\parallel = -0.14 \pm 0.01$ nm and $\delta^{\mathrm{phob}}_\perp = -0.10 \pm 0.01$ nm at the hydrophobic surface, showing a remarkable difference between the two surfaces: the dielectric interface is shifted toward the hydrophobic surface, $\delta^{\mathrm{phob}} < \delta^{\mathrm{phil}}$, indicating that water at this surface is a "better dielectric" than at the hydrophilic surface, when the reference is taken as z^{GDS}. However, this difference is more than compensated by the depletion layer, which is larger at the hydrophobic surface, so that $z^{\mathrm{DDS}}_{\perp\mathrm{phob}} > z^{\mathrm{DDS}}_{\perp\mathrm{phil}}$. In the following, we compare different ways of incorporating these dielectric effects into a coarse-grained model.

Poisson-Boltzmann (PB) modeling.—We consider a monovalent salt solution adjacent to a charged planar surface. Inspired by Eq. (2), we assume locality in the form $\varepsilon_0 E_\perp(z) = \varepsilon_\perp^{-1}(z) D_\perp(z)$, which is a good approximation when $D_\perp(z)$ varies slowly, i.e., at low salt concentration and low surface charge density σ_0 [6]. Taking the divergence of $E_\perp(z)$ and inserting $\nabla_z D_\perp(z) = P_0(z) = -2ec_0 \sinh[\beta e \psi(z)] \exp[-\mu(z)]$, with $\psi(z)$ the electrostatic potential and c_0 the bulk salt concentration, leads to the modified PB equation,

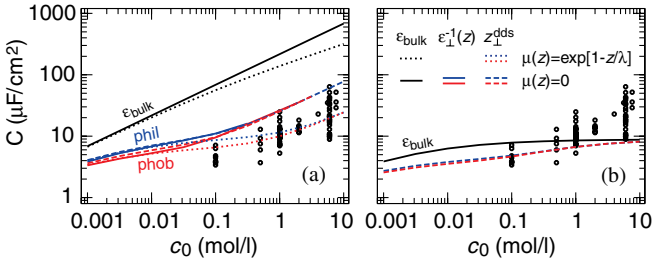

FIG. 3 (color online). Double-layer capacitance from Eq. (10) in the limit $\sigma_0 \to 0$, using $\varepsilon_\perp^{-1}(z) = \varepsilon_{\text{bulk}}^{-1}$ (black lines), $\varepsilon_\perp^{-1}(z)$ from MD (solid colored lines), and the sharp-kink-approximation using $z_\perp^{\text{DDS}}$ (broken lines). The blue lines correspond to hydrophilic and the red lines to hydrophobic surfaces. Circles denote experimental data [18]. (a) Surface charge σ_0 located at $z = 0$. The dotted lines include a soft ion repulsion $\mu(z) = \alpha \exp[1 - z/\lambda]$ and use $\varepsilon_{\text{bulk}}^{-1}$ (black) or the sharp-kink approximation (red and blue). (b) Surface charge located at $z = -0.1$ nm with $\varepsilon_\perp^{-1} = 1$ for $z < 0$, using $\varepsilon_\perp^{-1}(z) = \varepsilon_{\text{bulk}}^{-1}$ for $z > 0$ (solid line) and the sharp-kink approximation (dashed lines).

$$\varepsilon_0 \nabla_z^2 \psi = 2ec_0 \sinh[\beta e \psi] \exp[-\mu] \varepsilon_\perp^{-1} - D_\perp \nabla_z \varepsilon_\perp^{-1}, \tag{10}$$

where we used $\nabla_z \psi(z) = -E_\perp(z)$. The potential $\mu(z)$ contains all nonelectrostatic surface-ion contributions such as steric and solvation effects. The displacement field follows as $D_\perp(z) = \int_0^z P_0(z')dz'$, making Eq. (10) an integrodifferential equation [7,15].

Dielectric interface effects are most crucial for the surface capacitance, defined in differential form as $C = d\sigma_0/d\psi_0$ for $\sigma_0 \to 0$, where $\psi_0 = \psi(z = 0)$ is the surface potential. Figure 3(a) shows C calculated from Eq. (10) for different scenarios. For constant $\varepsilon_\perp^{-1}(z) = \varepsilon_{\text{bulk}}^{-1}$ with $\varepsilon_{\text{bulk}} = 71$ and $\mu(z) = 0$ (black solid line), the calculated C grossly overestimates experimental data (circles, for various surfaces and systems; see [18] for references), an observation that led Stern to postulate a low-dielectric surface layer [4]. Adding a generic soft ion repulsion, $\mu(z) = \alpha \exp[1 - z/\lambda]$, with λ of the order of the ionic radius, $\lambda = 0.15$ nm, and $\alpha = 1$, but keeping $\varepsilon_\perp^{-1}(z) = \varepsilon_{\text{bulk}}^{-1}$, does not improve the situation much (black dotted line, denoted $\varepsilon_{\text{bulk}}$), irrespective of the precise values of λ and α. On the other hand, the capacitance calculated using the full profiles $\varepsilon_\perp^{-1}(z)$ (colored solid lines, denoted by "phil" and "phob") agrees much better with experiments. Results of the sharp-kink approximation, $\varepsilon_\perp^{-1}(z) = \varepsilon_{\text{bulk}}^{-1}$ for $z > z^{\text{DDS}}$ and $\varepsilon_\perp^{-1}(z) = 1$ otherwise (broken lines), are very close to the full profile capacitance, explaining the success of the Stern layer concept and other, more refined expressions based on the width of the dielectric variation (for low salt concentration) [6,7]. Adding the soft ion repulsion $\mu(z)$ (colored dotted lines, only in conjunction with the sharp-kink approximation) leads to an excellent match with experiments even at high salt concentration. Note that experimentally, the capacitance increases only slightly with surface polarity [12,18], which is in line with our findings at hydrophobic and hydrophilic surfaces (red and blue lines in Fig. 3(a), respectively) and rationalized by the above-mentioned weak dominance of density depletion over interfacial dielectric effects on both surface types. The capacitance at very low salt concentration corresponds well to the value of 3.5 μF/cm^2 obtained for pure water at a platinum interface [21], despite the different water model used.

Note that the surface charge position at $z = 0$ corresponds to the outermost carbon layer on the hydrophobic surface and to the oxygen layer on the hydrophilic surface, a crucial detail motivated by surface chemical considerations [18]. Figure 3(b) shows the capacitance when the charge is displaced to $z = -0.1$ nm, using $\varepsilon_\perp^{-1}(z) = 1$ for $z < 0$. Solid lines are calculated using $\varepsilon_\perp^{-1}(z) = \varepsilon_{\text{bulk}}^{-1}$ for $z > 0$ and dashed lines using the sharp-kink approximation. Clearly, the dependence of the capacitance on the concentration deviates from the experimental trend in both cases, supporting our initial choice of the plane of charge position at $z = 0$.

In conclusion, we establish the framework to extract the full tensorial dielectric interface profiles from MD data. The perpendicular profiles $\varepsilon_\perp^{-1}(z)$ exhibit rich structure and distinct differences between hydrophobic and hydrophilic surfaces. In the context of coarse-grained PB modeling, experimental capacitance data are well reproduced. The dielectric dividing surface position is suggested as a straightforward definition of the width of a Stern layer with $\varepsilon = 1$. Modifications and nonlinear effects are expected at higher salt concentration, which shall be addressed in the future.

We thank the Deutsche Forschungsgemeinschaft for funding via Nanosystems Initiative Munich and project GE2214/1, and the Leibniz Rechenzentrum and FZ Jülich for computing time

[1] J. Israelachvili and H. Wennerström, Nature (London) **379**, 219 (1996).
[2] P. A. Bopp, A. A. Kornyshev, and G. Sutmann, J. Chem. Phys. **109**, 1939 (1998).
[3] J. Faraudo and F. Bresme, Phys. Rev. Lett. **92**, 236102 (2004).
[4] O. Stern, Z. Elektrochem. **30**, 508 (1924).
[5] K. J. Tielrooij *et al.*, Biophys. J. **97**, 2484 (2009).
[6] A. A. Kornyshev, W. Schmickler, and M. A. Vorotyntsev, Phys. Rev. B **25**, 5244 (1982).
[7] A. A. Kornyshev and M. A. Vorotyntsev, Can. J. Chem. **59**, 2031 (1981).
[8] L. Blum and D. Henderson, J. Chem. Phys. **74**, 1902 (1981).
[9] Y. Levin, Phys. Rev. Lett. **102**, 147803 (2009).
[10] A. A. Kornyshev, J. Electroanal. Chem. **204**, 79 (1986).

[11] J. Dzubiella, J. M. J. Swanson, and J. A. McCammon, Phys. Rev. Lett. **96**, 087802 (2006).
[12] Y.-T. Kim *et al.*, Appl. Phys. Lett. **87**, 234106 (2005).
[13] S. Marčelja *et al.*, J. Chem. Soc., Faraday Trans. 2 **73**, 630 (1977).
[14] A. Abrashkin, D. Andelman, and H. Orland, Phys. Rev. Lett. **99**, 077801 (2007).
[15] F. Paillusson and R. Blossey, Phys. Rev. E **82**, 052501 (2010).
[16] F. H. Stillinger and A. Ben-Naim, J. Chem. Phys. **47**, 4431 (1967).
[17] V. Ballenegger and J.-P. Hansen, J. Chem. Phys. **122**, 114711 (2005).
[18] See Supplemental Material at http://link.aps.org/supplemental/10.1103/PhysRevLett.107.166102 for the details of the experimental data displayed in Fig. 3 and derivations of some of the equations used in the main text.
[19] C. Sendner *et al.*, Langmuir **25**, 10768 (2009).
[20] M. R. Reddy and M. Berkowitz, Chem. Phys. Lett. **155**, 173 (1989).
[21] G. Nagy, K. Heinzinger, and E. Spohr, Faraday Discuss. **94**, 307 (1992).